High-Speed EML and Assembly Techniques for GPU Cluster System

M. Shirao, *Member, IEEE*, T. Fujita, A. Uchiyama, *Member, IEEE*, S. Okuda, T. Nagamine, K. Abe, and N. Ohata

***Abstract*— In this paper, we present the development of high-speed Electro-Absorption Modulated Laser Diodes (EMLs) and advanced assembly techniques tailored for GPU cluster systems. The increasing computational demands driven by generative AI and large language models necessitate significant advancements in data transfer speeds within data centers. We introduce a high-mesa structure for the Electro-Absorption Modulator (EAM) within the EML, achieving superior modulation efficiency and bandwidth. The EML is designed for 400 Gbps/lane modulation, addressing the need for higher data rates such as 3.2 Tbps pluggable transceivers. To achieve 400 Gbps/lane, we fabricated and demonstrated EMLs with narrow mesa widths of 1.1 μm and 0.8 μm in the high mesa structure. Achieving 400 Gbps requires a modulation bandwidth exceeding 100 GHz, which poses a significant challenge to the assembly. We propose an advanced EML assembly that includes a Glass-AlN hybrid submount to overcome these limitations. This hybrid submount significantly reduces the parasitic inductance of the wire bonding and enables the adoption of low dielectric material for RF trace, achieving higher modulation bandwidth. Our prototype demonstrates a 3 dB bandwidth exceeding 100 GHz, both numerically and experimentally. Additionally, targeting Near Package Optics (NPO) and Co-Packaged Optics (CPO) with high edge density, we investigate packaging technology that eliminates the need for wire bonding. Our prototype demonstrated a 3 dB bandwidth of 85 GHz and a clear eye opening for 113.4 GBaud PAM4 signals. These innovations pave the way for future high-density photonics-electronics convergence technologies, essential for next-generation optical interconnects in high-performance computing environments.**

***Index Terms*—EML, EA-DFB, EAM, modulator, PAM4, CPO, 400G, 3.2T, interconnection,**

I. INTRODUCTION

Optical communication technology is gaining importance in data centers and high-performance computing infrastructure. Improving data transfer speeds in GPU cluster systems directly correlates with maximizing computational capabilities. The emergence of generative AI, represented by large language models (LLMs), has recently led to an explosive increase in the computational requirements for machine learning. The number of parameters used in machine learning has increased approximately 400 times every two years [1]. For instance, OpenAI's GPT-3 uses 175 billion parameters, while models like Switch Transformer and GPT-4 use over a trillion parameters. On the other hand, the computational performance of processors has only been improving at a rate of about 2.6 times every two years, and the interconnect bandwidth required for computing has been increasing at a rate of about 1.4 times every two years. Consequently, thousands of GPUs are connected in parallel to form clusters to enhance computational performance and execute machine learning significantly. There are two main approaches to evolving GPU systems: scale-up and scale-out. For scale-up, massive GPUs are connected in an all-to-all manner within a rack to form a single virtual giant GPU. Thousands of cost-effective copper cables are currently used for this purpose, but with future speed increases, optical fiber connections are anticipated [3-5]. For scale-out, i.e., parallelizing GPU racks, an optical fiber link is used for inter-rack communication, and pluggable transceivers are commonly employed [6]. Specifically, 1.6T-DR8 transceivers that employ 8 × 200 Gbps are mainstream, and re-use of the DR8 configuration, that is 8× 400 Gbps, is expected for 3.2T transceivers [7]. This approach achieves high bandwidth without increasing the number of optical components or fibers. Co-packaged optics (CPO) is also expected to be introduced to the GPU system, particularly for network switches, as indicated at GTC 2025 [8].

To achieve the 400 Gbps required for pluggable transceivers, 200 GBaud PAM4 (Pulse Amplitude Modulation 4-level) is the most promising, which requires a bandwidth exceeding 100 GHz for modulators. Multiple technologies are considered candidates for optical modulators to achieve 400 Gbps. Silicon photonics modulators offer high-density integration and have a strength in multi-lane configurations compared to other candidates. Practical implementation towards 200 Gbps is progressing, and a bandwidth of nearly 90 GHz has been reported to achieve 400 Gbps [9, 10]. Silicon Organic Hybrid (SOH) modulators are also being actively researched to go beyond the limit of silicon photonics modulators [11]. Thin-Film Lithium Niobate (TFLN) modulators, having traveling-

Manuscript is submitted on xx, 2025.

This paper is based on results obtained from the project, "Research and Development Project of the Enhanced Infrastructures for Post-5G Information and Communication Systems" (JPNP20017), commissioned by the New Energy and Industrial Technology Development Organization (NEDO).

M. Shirao, A. Uchiyama and N. Ohata are with Information Technology R&D Center, Mitsubishi Electric Corporation, 5-1-1, Ofuna, Kamakura, Kanagawa, 247-8502, Japan

(email: Shirao.Mizuki@db.mitsubishielectric.co.jp).

A. Uchiyama, and S. Okuda are with High Frequency and Optical Device Works, Mitsubishi Electric Corporation, 4-1, Mizuhara, Itami, Hyogo, 664-8641, Japan.

T. Nagamine is with Manufacturijng Engineering Center, Mitsubishi Electric Corporation, 8-1-1, Tsukaguchihonmachi, Amagasaki-shi, Hyogo 661-8661, Japan

K. Abe is with Advanced Technology R&D Center, Mitsubishi Electric Corporation, 8-1-1, Tsukaguchi-honmachi, Amagasaki, Hyogo, 661-8661, Japan.

wave electrode structures, have reported bandwidths exceeding 100 GHz [12-14]. Various studies are being conducted to improve modulation efficiency using transparent electrodes and to compensate for bandwidth in the optical domain [14]. However, their large footprint is still a challenge. We consider Electro-Absorption Modulated Integrated Laser Diodes (EMLs), having a small footprint and a low modulation voltage capability of less than 1.0 Vpp, thanks to the highly efficient quantum-confined Stark effect (QCSE) of III-V semiconductor, to be the preferable choice for 400 Gbps applications, as multiple reports exist on high-speed EMLs beyond 100 GHz [15-17]. Differential driving has also been explored to enhance noise resistance and reduce driver output voltage [18, 19]. The EML is conventionally mounted on an aluminum nitride (AlN) submount and assembled using a wire bonding technique. However, at frequencies exceeding 100 GHz, parasitic inductance caused by the wire bonding limits bandwidth, necessitating advanced packaging technologies to overcome this.

This paper introduces a unique high-mesa structure for the Electro-Absorption Modulator (EAM) in the EML, providing a superior trade-off between operation speed and modulation voltage [20]. Then, the progress in the EML development will be discussed, targeting 400 Gbps [17]. Next, efforts should be made to minimize the parasitic inductance and break through the assembly limit to achieve bandwidth beyond 100 GHz. Advanced packaging configurations that do not use wire bonding to achieve higher edge density, such as CPOs, are also discussed. The presented data in this paper are partially included in the abstract of OFC 2025 [21] with additional data and in-depth discussion.

II. EML Chip Development

Fig. 1 illustrates the structure of our EML, which integrates a Buried Heterostructure Distributed Feedback Laser Diode (DFB-LD) for high optical output power, an EAM, and a spot-size converter to obtain the beam with a far-field pattern of less than 20° (FWHM) in both the vertical and horizontal axes. A high-mesa EAM was incorporated into the EML design to achieve superior modulation efficiency. In the EAM section, the propagating light is strongly confined within the optical absorption layer due to the low-refractive-index cladding (insulator) on both sides of the mesa. The high-mesa structure ensures the preservation of a favorable waveguide mode even at a narrowed mesa width, i.e. it facilitates a reduction in the mesa width, thereby decreasing electrostatic capacitance while maintaining a high optical confinement factor. This structure has enabled excellent performance at 112.5 GBaud PAM4 and up to 10 km transmission, shown in Fig. 2 [22]. We have also reported the bandwidth enhancement from 67 GHz to 85 GHz by narrowing the mesa width from 1.4 µm to 1.1 µm. An excellent eye diagram at 155 GBaud PAM4 with a TDECQ value of 3.3 dB was successfully demonstrated as shown in Fig. 3 (a) [23]. Note that all measurements presented in this paper were conducted using an RF probe directly contacted onto the submount. A raised cosine-shaped data pattern (SSPRQ) was generated using an arbitrary waveform generator (AWG, Keysight M8199) and amplified to the required modulation amplitude with a bias tee integrated electrical amplifier (SHF, M827B). The calibration of the measurement setup was performed just before the RF probe. The evaluations of small-signal characteristics were conducted using an optical component analyzer, and the optical eye diagrams were captured using a sampling oscilloscope. After passing through a fourth-order Bessel-Thomson filter, the signals underwent FFE processing for TDECQ evaluation. During the evaluation, the EML was temperature-controlled using a thermoelectric cooler (TEC). Further bandwidth enhancement is expected by reducing the electrostatic capacitance of the EAM. However, reducing the mesa width poses challenges for the fabrication. We have achieved a mesa width of less than 1 µm by strictly controlling the process conditions. To enhance mechanical strength and facilitate electrode formation on the very narrow mesa, both sides of the mesa are filled with a low-refractive-index insulating material. Although narrowing the mesa width could potentially lead to mechanical fragility, no destruction of the waveguide structure was observed during the process for the EML fabrication with a width of W = 0.8 µm. Fig. 3 shows the 155 GBaud PAM4 optical eye diagrams of the EML with a mesa width of 0.8 µm. The electrostatic capacitance is reduced by approximately 30%, improving the TDECQ value from 3.3 dB to 2.4 dB for a 155 GBaud PAM4 signal [17]. In practice, narrowing the mesa width increases resistance, which can lead to a decrease in bandwidth. However, within the range of mesa widths examined in this study, we have observed an improvement in bandwidth. By reducing resistance through adjusting parameters such as doping concentration, further bandwidth enhancements can be expected. It should be also noted that the improvement is attributed not only to the low capacitance but also to the advanced assembling technique discussed in the next chapter.

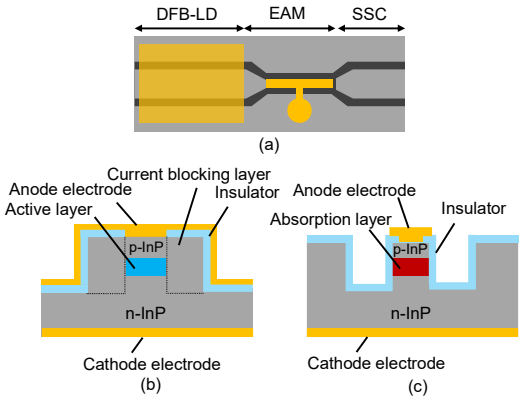

Fig. 1 An EML employing high-mesa EAM. (a) top view of EML, (b) cross-sectional view of BH DFB-LD, (c) cross-sectional view of high-mesa EAM

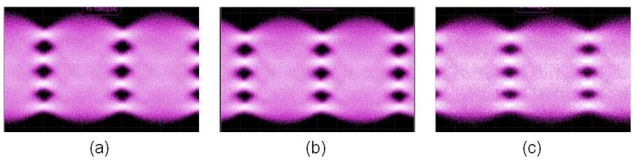

Fig. 2 Transmission test results over standard single-mode fiber using an EML (W = 1.1 µm) operating at 1311.6 nm for 112.5 GBaud PAM4. (a) back-to-back with TDECQ = 1.43 dB and extinction ratio (ER) = 4.5 dB, (b) 2 km with TDECQ = 1.44 dB, (c) 10 km with TDECQ = 1.57 dB.

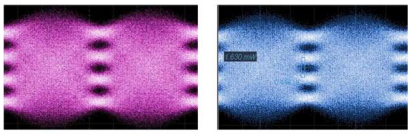

Fig. 3 Optical eye diagrams for 0.8 Vpp, 155 GBaud PAM4 electric signal. TDECQ calculation was undertaken with target SER at 9.7E-3. (a) mesa width W = 1.1 µm with TDECQ = 3.3 dB and ER = 3.0 dB, (b) W = 0.8 µm with TDECQ = 2.4 dB and ER = 2.9 dB.

III. Short Wire Assembly

Fig. 4 (a) shows the schematic diagram around the EAM of the EML assembly. The EML is mounted on an AlN submount using AuSn solder. The AlN has excellent heat dissipation properties and a thermal expansion coefficient of 4.6×10^{-6} /K, equivalent to InP devices. Therefore, from the perspective of stress reduction on the EML, AlN is suitable as a submount material. The electrical signal output from the signal source is propagated to the EAM via the RF trace formed on the AlN submount and the 1st wire, then connected to the termination resistor via the 2nd wire. The 2nd wire has an inductance element, resulting in high impedance for the high-frequency signal and exhibiting a peaking effect. The equivalent circuit model related to the EAM is shown in Fig. 4 (b). It is clear that the 1st wire gives a parasitic inductance, which causes a limitation of the modulation bandwidth. The parasitic inductance increases with the length of the 1st wire L as shown in Fig. 5. Fig. 5 shows the small signal response for various L within the range from 600 µm to 300 µm. In this simulation, the electrostatic capacitance of the EAM was set to 60 fF. The minimum value of L = 300 µm is assumed to be the shortest physical distance required for wire bonding from the AlN submount to the bonding pad on the top surface of the approximately 100-µm-thick EAM. At L = 600 µm, the 3 dB bandwidth is 60 GHz; however, as L decreases, the parasitic inductance is reduced, and a bandwidth of 85 GHz is expected at L = 300 µm. These results suggest that new approaches are necessary to improve the modulation bandwidth further. Therefore, we investigated a hybrid submount that combines multiple substrates to shorten the wire length.

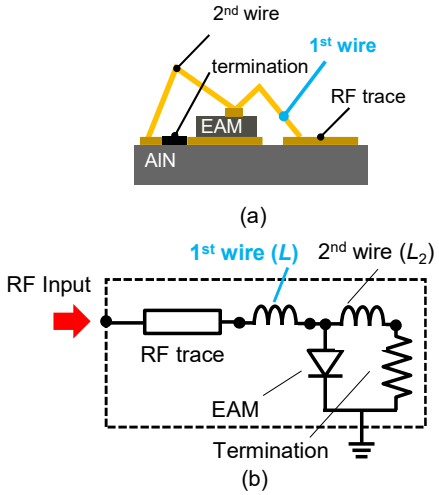

Fig. 4 Schematic diagram around the EAM of the EML assembly. (a) cross-sectional view of EAM on the AlN submount. (b) A simplified circuit model of the EML and submount.

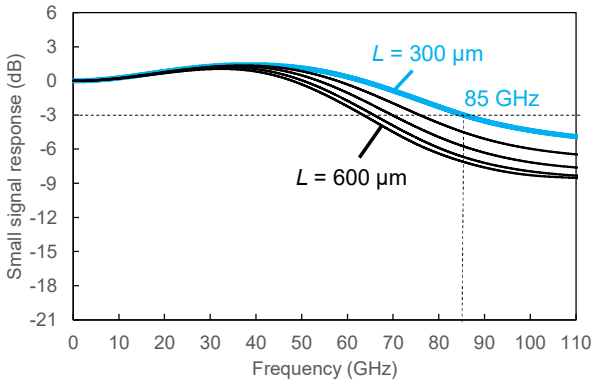

Fig. 5 Small signal responses of EML on submount for various 1st wire lengths at the EAM mesa width W = 1.1 µm. Small-signal responses was calculated using a 3D electromagnetic field simulator (HFSS) for the submount and wire bonding. The extracted S-parameters from the 3D model were combined with the equivalent circuit model of the EAM [22] in a circuit simulator. The length of the second wire was fixed at approximately 600 µm.

A. A Stepped Submount Combining Multiple AlN Chips

This section describes the stepped submount designed to shorten the 1st wire length, in which the concept has been reported [24]. In Fig. 4, the configuration involved bonding wires from the surface of the AlN submount to the bonding pads of the EAM. Therefore, achieving a 1st wire length of less than 300 µm was challenging due to physical distance. Fig. 6 shows a submount that allows for shorter 1st wire lengths. This configuration combines a carrier for mounting the EML and an RF sub for forming an RF trace (Model A) as shown in Fig 7. Both the carrier and the RF sub are made of AlN. By making the thickness of the RF sub equal to that of the EML, the 1st wire can be shortened to approximately 100 µm, thereby reducing parasitic inductance. The RF sub is side-metallized, electrically connecting the GND pattern of the RF trace with the cathode (the back side of the EML).

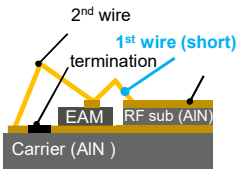

Fig. 6 Cross-sectional view of EAM on stepped submount using multiple AlN chips.

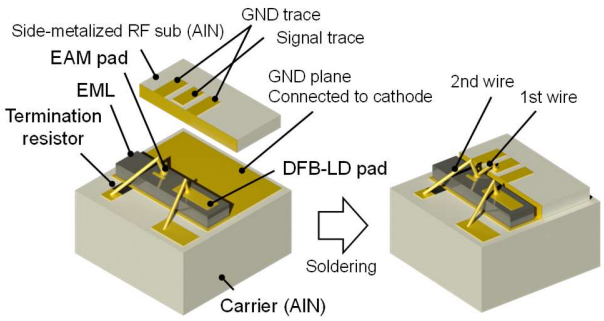

Fig. 7 Structure of stepped submount with GND plane (Model A)

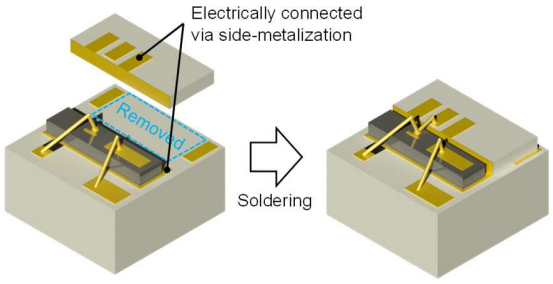

Fig. 8 Structure of stepped submount without GND plane (Model B)

The black plot in Fig. 9 shows the simulation result of the signal response of Model A. While a flat characteristic is obtained up to 80 GHz, a strong resonance is observed at 90 GHz. This resonance originates from the ground on the backside of the RF substrate, behaving as a stub. Such resonance can cause critical degradation of eye quality for 400 Gbps modulation. Therefore, as shown in Fig. 8, we adopted a configuration where the GND plane is removed under the RF trace (Model B) to avoid the resonance related to the GND plane. Metal patterns for AuSn solder formation are retained in areas away from the RF trace, so the ground pattern of the RF sub and the back side of EML (cathode) are electrically connected. Although not shown in the figure, the back side of the RF sub also has the metal pattern partially removed, the same as the carrier. This forms a GSG coplanar line on the RF sub. The RF sub is side metallized similarly to Model A, electrically connecting the cathode on the back side of the EML with the GND traces. By adopting this configuration, the resonance at 90 GHz can be eliminated, as shown in Fig. 9, and the modulation bandwidth can be improved to 92 GHz compared to the 85 GHz shown in Fig. 5.

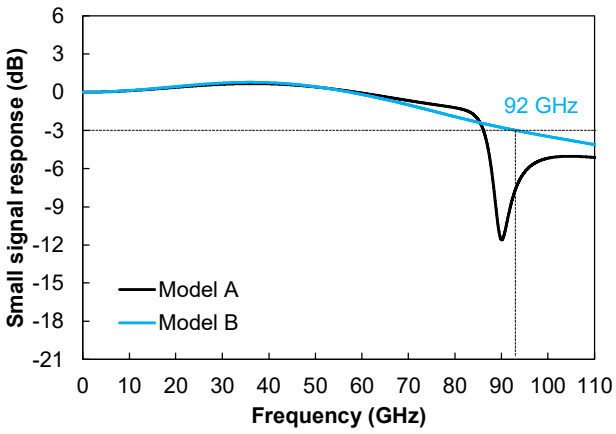

Fig. 9 Small signal responses of EML on stepped submount. The black plot indicates a stepped submount with a GND plane on the carrier (Model A). Blue plot describes without the GND plane (Model B).

B. A Glass-ALN Hybrid submount

Adopting low dielectric constant materials, e.g., glass materials, improves modulation bandwidth. It reduces parasitic capacitance and shifts the resonance frequency to higher, thanks to the longer electrical length or wavelength in the low dielectric constant medium. We have previously reported a submount made of a glass material with a dielectric constant of 3.8, with inferior heat dissipation properties. Introducing thermal vias enables excellent heat dissipation performance equivalent to AlN [25]. However, compared to AlN substrates, which have a thermal expansion coefficient matching that of InP devices, low dielectric constant materials have a single-digit larger thermal expansion coefficient. This discrepancy imposes unintended stress on the EML, leading to issues such as kinks in the P-I curve and degradation of the reliability.

To leverage the advantages of low dielectric constant materials while avoiding adverse effects on EML operation, we propose a Glass-AlN hybrid submount configuration, as shown in Fig. 10 [25]. The EML is mounted on a carrier made of AlN, which has excellent heat dissipation and a small difference in thermal expansion coefficient from InP devices. Adjacent to the EML, an RF sub made of quartz glass is mounted. The RF sub is also side-metallized and has a GND plane beneath the RF trace removed, the same as the Model B in Fig. 8, to suppress resonance. By fabricating the RF sub thickness of 100 μm, the length of the 1st wire is minimized. This configuration allows us to simultaneously achieve excellent heat dissipation, high reliability for the EML, and the superior high-frequency characteristics of low dielectric constant materials for the RF trace. Fig. 11 shows the simulation results of the small-signal response of the EML mounted on a glass-AlN hybrid submount. Using quartz glass for the RF sub, a modulation bandwidth of 106 GHz, an improvement of 14 GHz over that of the AlN sub (Fig. 9), was achieved.

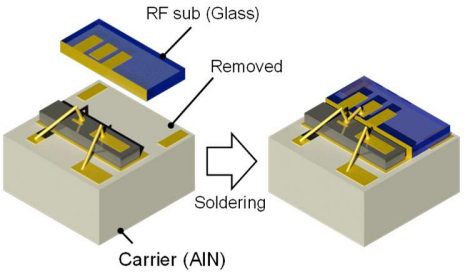

Fig. 10 Structure of glass-AlN hybrid submount (Model C)

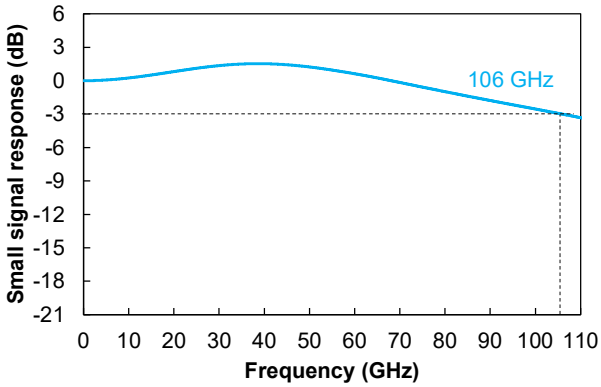

Fig. 11 Small signal response of EML on glass-AlN hybrid submount (Model C).

IV. Fabrication

This section describes the evaluation results of the prototype EML assembly mounted on a Glass-AlN hybrid submount. Based on the concept shown in Fig. 10, we fabricated the carrier (AlN) and RF sub (quartz glass). They were assembled using AuSn solder and wire bonding. Fig. 12 shows a side view of the prototype. It can be observed that the glass sub and EML are mounted closely on the AlN sub. The thickness of the glass sub is 100 µm, equivalent to that of the EML, so that the length of the 1st wire can be shortened to approximately 100 µm. Fig. 13 shows the optical output characteristics at an LD temperature of 50 °C using an EAM with a mesa width of 0.8 µm. No output saturation or kinks were observed since the EML is mounted on an AlN substrate, which poses low reliability risks. The spectral characteristics in Fig. 14, with an LD current of 80 mA and an LD temperature of 50 °C, also confirm excellent performance with a side mode suppression ratio (SMSR) of over 50 dB.

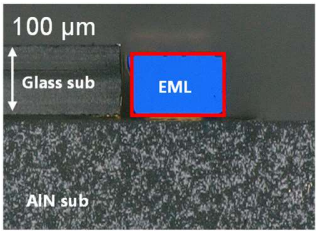

Fig. 12 Side view of EML on glass-AlN hybrid submount

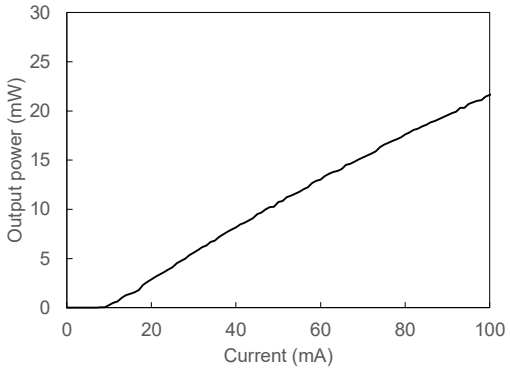

Fig. 13 P-I characteristics of EML on glass-AlN hybrid submount at LD temperature of 50 °C.

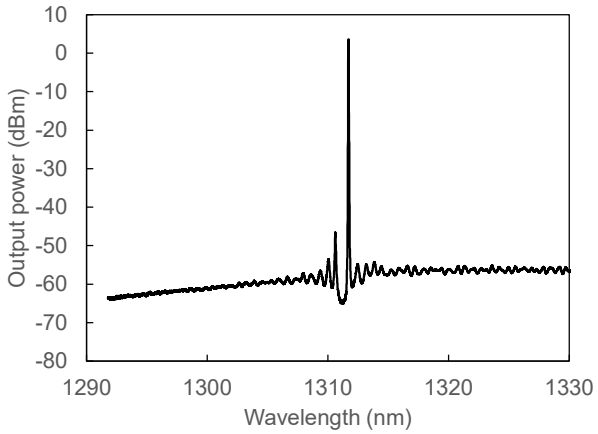

Fig. 14 Spectrum characteristics of EML on glass-AlN hybrid submount at LD temperature of 50 °C.

Fig. 15 compares the small signal responses of EMLs with EAM mesa widths of 1.1 µm and 0.8 µm, mounted on Glass-AlN hybrid submounts. For the EAM with a mesa width of 1.1 µm, which is estimated to have a capacitance of 60 fF, a modulation bandwidth of 100 GHz was achieved experimentally. This result is almost consistent with the simulation result of 106 GHz shown in Fig. 11. By reducing the mesa width to 0.8 µm and lowering the EAM capacitance to approximately 42 fF, an excellent modulation bandwidth exceeding the measurement limit of 110 GHz was successfully obtained. A peak appears at 40 GHz in Fig. 11 and around 20 GHz in Fig. 15, indicating a higher peaking level. The peaking frequency mainly depends on the 2nd wire length and the RC time constant of the EA modulator. The higher peaking in Fig. 15 likely results from differences between simulation and experiment, or variations in wire length. The RC time constant seems to cause decline in small signal response at lower frequencies in Fig. 15 than in Fig. 11, suggesting a minor mismatch between evaluated EML and our device model. However, given that a clear bandwidth improvement has been confirmed compared to previous reports [22], the effectiveness of the proposed assembling technique is evident. It should be noted that the frequency response irregularities above 80 GHz, originating from the measurement setup, were observed, indicating a certain degree of error in estimating the modulation bandwidth. Therefore, the modulation bandwidth was estimated, ignoring tiny dips in the frequency response.

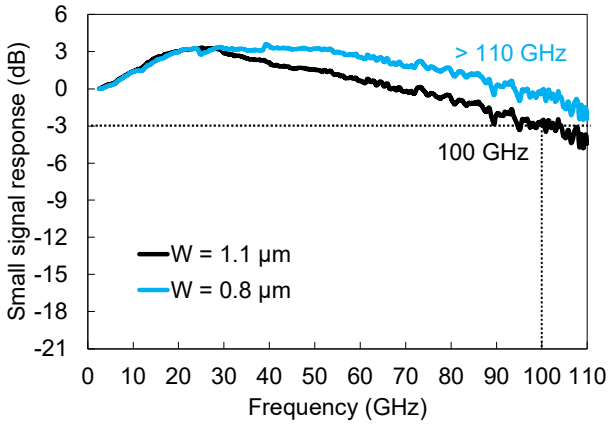

Fig. 15 I-V and P-I characteristics of EML on glass-AlN hybrid submount

V. EML Assembly For Higher Edge Density

We discussed the EML assembly techniques for pluggable transceivers using wire bonding in previous chapters. Considering the photonics-electronics convergence technology required for NPOs/CPOs with high edge density, developing packaging technology that does not use a relatively large footprint wire bonding technique is essential. Fig. 16 shows examples of packaged EML configurations for such applications. Although the integration density of the EML is not as high as that of an advanced semiconductor foundry process, which combines electronic integrated circuit (EIC) and

photonic integrated circuit (PIC) [8], the EIC can be flip-chip mounted on top of the EML based on a junction-up configuration in Fig. 16 (a), leading to 3D packaging technology. Fig. 16 (b) shows a junction-down configuration. Since the EIC and EML are mounted side by side, this configuration corresponds to 2D or 2.5D packaging technology. In this report, we fabricated a prototype shown in Fig. 17 to mimic the junction-up configuration that propagates electric signals directly from the RF substrate without wire bonding. Typically, the EML has the cathode on the back side and the anode on the surface. Therefore, a pair of GND blocks, having the same thickness as the EML, was placed on both sides of the EML to enable cathode contact from the top surface. A maximum height misalignment of up to 10 µm can occur between the EML and GND blocks. To compensate for the observed lower EML height, we stacked two Au stud bumps on the EML and one on the GND blocks to align their heights. This trial was conducted with a single channel. However, as the EML and GND blocks have a width of 0.2 mm and a 50 µm gap, an optical pitch of 500 µm can be achieved by arraying the same chips. Next, an RF sub made of quartz glass was directly bonded to the EML via Au stud bumps. Evaluation was undertaken by direct contact of the RF probe on the RF sub. The termination resistor and peaking inductors of the EAM are monolithically integrated onto the glass substrate. Fig. 18 shows a top view of the prototype, where the GND blocks are placed on both sides of the EML, and the RF sub made of quartz glass can be seen on top. Fig. 19 shows the evaluation results of the prototype. An EML at a temperature of 50 °C achieved a 3 dB bandwidth of 85 GHz. Approximately 100 GHz bandwidth is achieved in Fig. 15, while only 85 GHz bandwidth is obtained in Fig. 19. In Fig. 15, the approximately 100-µm-long 1st wire was formed in air ($\varepsilon = 1$).

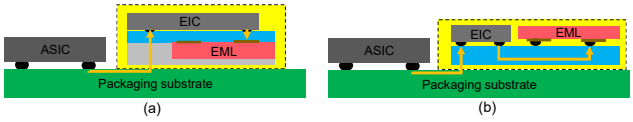

Fig. 16 Examples of EML assembly in high edge density applications. (a) junction-up configuration. (b) junction-down configuration.

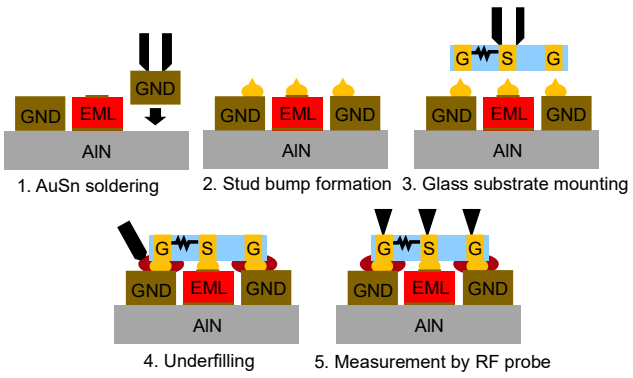

Fig. 17 Fabrication process of the prototype based on the junction-up configuration.

On the other hand, Fig. 19 utilizes a 100-µm-long metal-filled via traversing a quartz substrate ($\varepsilon = 3.8$), together with double-stacked Au stud bumps on the EML, which increases the parasitic inductance and thus lowers the bandwidth compared to the wire bonding in Fig. 15. Increasing the via diameter may mitigate this effect and enhance bandwidth. Moreover, wire-bonding-less assembly offers significant advantages for both high-frequency performance and increased integration density. The TDECQ value and extinction ratio for a 113.4 GBaud PAM4 signal with a modulation voltage of 1.0 Vpp were estimated to be 1.8 dB and 4.9 dB, respectively.

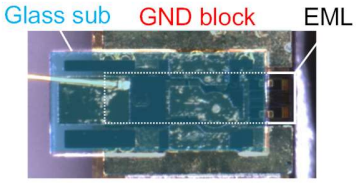

Fig. 18 Top view of the prototype.

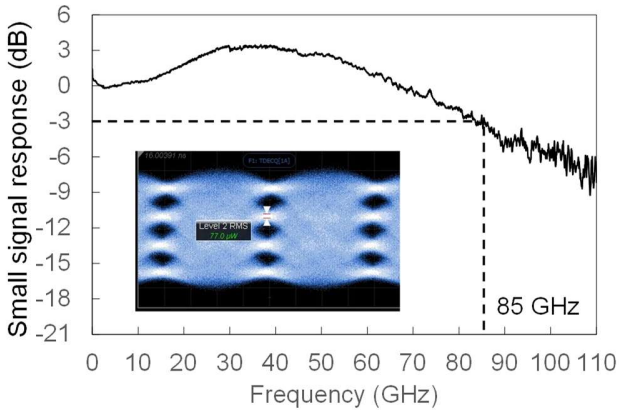

Fig. 19 Evaluation result of the prototype using an EML with a mesa width of 1.1 µm. Small signal response and optical eye diagram at 113 GBaud PAM4 (inset figure).

VI. Conclusion

This paper discusses the development status of high-speed EML and its advanced assembly technique, aiming to achieve 400 Gbps/lane. The mesa width of the high-mesa EAM was shrunk as narrow as 0.8 µm for reducing electrostatic capacitance. A Glass-AlN hybrid submount that combines a thermally and mechanically reliable AlN carrier and a low-dielectric quartz glass RF sub was proposed as an EML assembly to prevent degradation of modulation bandwidth. Since the hybrid structure reduces parasitic inductance caused by wire bonding, we successfully demonstrated modulation bandwidths exceeding 100 GHz in prototypes with EMLs having mesa widths of 1.1 µm and 0.8 µm. Additionally, we explored packaging technologies that eliminate the need for wire bonding for applications requiring high edge density, such as NPO and CPO. In a junction-up configuration prototype, we realized a structure directly connecting electrical signals from the quartz glass RF sub to the EAM without wire bonding, achieving a 3 dB bandwidth of 85 GHz and a clear eye opening

for 113.4 GBaud PAM4. These innovations provide a robust foundation for next-generation photonics-electronics convergence technology, essential for high-performance optical interconnects.

REFERENCES

[1] https://medium.com/riselab/ai-and-memory-wall-2cb4265cb0b8.
[2] https://www.nvidia.com/ja-jp/data-center/nvlink/
[3] Universal Chiplet Interconnect Express, UCIe 1.0 Specification
[4] R. Baghdadi, et al., "Monolithically Integrated Microring Transmitter and Receiver for High-Density 3D Co-Packaged Optics," Tu3J.6, OFC2025
[5] P. Bhargava, et al., "A UCIe Optical I/O Retimer Chiplet for AI Scale-up Fabrics," Th4B.3, OFC2025.
[6] M. G. Saber and Z. Jiang, "Physical Layer Standardization for AI Data Centers: Challenges, Progress and Perspectives," in IEEE Network, doi: 10.1109/MNET.2025.3557812.
[7] H. V. Habi and H. Messer, "Recurrent neural network for rain estimation using commercial microwave links," *IEEE Trans. Geosci. Remote Sens.*, vol. 59, no. 5, pp. 3672-3681, May 2021.
[8] J. Huang, GTC 2025 Keynote, Available: https://www.nvidia.com/ja-jp/on-demand/session/gtc25-s72484/
[9] J. Xue, et al., "An 8×256 Gbps Silicon Photonic DWDM Transmitter with Thermally Stable Microring Modulators," Th1E.3, OFC2025
[10] H. Wang, et al, "90 GHz Silicon Mach-Zehnder Modulator with Integrated Equalizer for 1.6 Tbps (200G/λ) IMDD Transceivers," M2K.1, OFC2025
[11] A. Schwarzenberger, et al., "Silicon-Organic Hybrid (SOH) Mach-Zehnder Modulator (MZM) for Single-Carrier IMDD Line Rates of 500 Gbit/s and Beyond," M4K.1, OFC2025
[12] X Meng, et al., "Thin-Film Lithium Niobate Modulators with Ultra-High Modulation Efficiency," M3K.2, OFC2025
[13] Y. He, et al., "Dual-Band 390 Gbps High Coupling Efficiency Thin Film Lithium Niobate Modulator With 3-dB Bandwidth Exceeding 110 GHz," Tu2J.4, OFC2025
[14] Y. Yamaguchi, et al., "Fully Packaged 100-GHz-Bandwidth EO-Equalizer-Integrated TFLN Modulator With Record-High Slope Efficiency Enabling 200-GBaud Signaling," Th4D.4, OFC2025
[15] H. Asakura et al., "400 Gbps Semi-Cooled Lumped-Electrode EA-DFB Laser Operating At 200 Gbaud PAM4 Modulation With 0.6 Vpp," ECOC 2024, Th3A.1, 2024.
[16] P. Bhasker, et al., "413 Gbits/s PAM-6 O-Band CWDM Electroabsorption Modulated Lasers for 400G per Lane IM-DD Applications," Tu2J.2, OFC2025
[17] S. Okuda, et al., "High-Speed 340 Gbps PAM4 and 450 Gbps PAM6 Operations of Narrow High-Mesa EML," Tu2J.7, OFC2025
[18] Z. Zhang, et al., "Differential Drive EML with P/N Electrode Isolated Toward Low Vpp Application," M3K.6, OFC2025
[19] S. Ohno, et al., "226 Gbps PAM4 Operation Using Differential Drive EA-DFB Laser With 2.0-Vppd Swing Over 10-km SSMF Transmission for 1.6TbE Transceivers," M4K.6, OFC2025
[20] Y. Morita et al., "1.3 μm 28 Gb/s EMLs with hybrid waveguide structure for low-power-consumption CFP2 transceivers," 2013 Optical Fiber Communication Conference and Exposition and the National Fiber Optic Engineers Conference (OFC/NFOEC), Anaheim, CA, USA, 2013, pp. 1-3.
[21] M. Shirao, et al., "High Speed EML and Assembly Techniques for GPU Cluster System," Tu2J.3, OFC2025
[22] A. Uchiyama et al., "Demonstration of 155-Gbaud PAM4 and PAM6 Using a Narrow High-Mesa Electro-Absorption Modulator Integrated Laser for 400 Gb/s Per Lane Transmission," in Journal of Lightwave Technology, vol. 43, no. 4, pp. 1868-1873, 15 Feb.15, 2025
[23] A. Uchiyama et al., "225 Gb/s PAM4 2 km and 10 km Transmission of Electro-Absorption Modulator Integrated Laser With Hybrid Waveguide Structure for 800 Gb/s and 1.6 Tb/s Transceivers," in Journal of Lightwave Technology, vol. 42, no. 4, pp. 1225-1230, 15 Feb.15, 2024
[24] T. Fujita, A. Uchiyama, S. Okuda, M. Shirao, and N. Ohata, "Fabrication of a Glass Submount with High Heat Dissipation," 2024 IEEE CPMT Symposium Japan (ICSJ), Kyoto, Japan, 2024, pp. 128-131
[25] K. Naoe, "Ultrahigh Speed EA-DFB Lasers beyond 200 Gbps per Lane," in Optical Fiber Communication Conference (OFC) 2023, Technical Digest Series (Optica Publishing Group, 2023), paper M2D.1.
[26] M. Shirao, S. Okuda, T. Fujita, N. Ohata, "Beyond 100GHz operation of AlN-glass hybrid submount for high-speed EML assembly," Proc. SPIE 13374, Next-Generation Optical Communication: Components, Sub-Systems, and Systems XIV, 133740D (19 March 2025)

M. Shirao (Member, IEEE) Mizuki Shirao received his B.E., M.E., and Ph.D. in Electrical and Electronic Engineering from Tokyo Institute of Technology in 2007, 2009, and 2011, respectively. He joined the Information Technology R&D Center, Mitsubishi Electric Inc., in Kanagawa, Japan 2011. He engaged in research and development of optical devices for high-speed Ethernet modules and the standardization of IEEE 802.3 400 GbE. In 2019, he joined the University of California, Berkeley, as a visiting researcher and engaged in research on photonic integrated circuits. In 2021, he joined the Information Technology R&D Center, Mitsubishi Electric Inc. His research interests include high-speed optical devices, photonic integrated circuits, and their related assembly/packaging technique.

Asami Uchiyama received her B.S. and M.S. degrees in Condensed Matter Physics from Tokyo Institute of Technology, Tokyo, Japan, in 2010 and 2012, respectively. She joined Mitsubishi Electric Corp. in 2012. She is currently with High Frequency and Optical Device Works, Mitsubishi Electric Corp., in Hyogo, Japan, where she has been developing high-speed semiconductor optical devices for optical communication.

Shinya Okuda received his B.E. and M.E degrees in Electrical, Electronic, and Information Engineering from Osaka University in 2014 and 2016, respectively. He joined High Frequency and Optical Device Works, Mitsubishi Electric Corp., in Hyogo, Japan, in 2016.

Kenichi Abe received his B.S. and M.S. degrees in Applied Physics from Tokyo Institute of Technology, Tokyo, Japan, in 1996 and 1998, respectively. He joined Mitsubishi Electric Corp. in 1998. He is with the Advanced Technology R&D Center, Mitsubishi Electric Corp., in Hyogo, Japan.

N. Ohata received the B.E., M.E., and Ph.D. degrees in innovation systems engineering from Utsunomiya University, Utsunomiya, Japan, in 2004, 2006, and 2017, respectively. In 2008, he joined Mitsubishi Electric Corporation, Tokyo, Japan, and has been working on the research and development of high-speed optoelectronic devices for optical fiber communication. Dr. Ohata is a member of the Institute of Electronics, Information, and Communication Engineers, Japan.